

## Article

# Synthesis, Analysis, and Characterization of Aluminum Nanoparticles Coated with 2,2,4-Trimethylpentane

Guanyi Wang<sup>1</sup>, Huixin Wang<sup>1</sup>, Qingzhong Cui<sup>1,\*</sup>, Xiaoping Li<sup>2</sup>, Xingyu Wu<sup>3</sup>, Hongzhe Liao<sup>1</sup> and Zhe Zhang<sup>1</sup>

<sup>1</sup> State Key Laboratory of Explosion Science and Technology, Beijing Institute of Technology, Beijing 100081, China

<sup>2</sup> Shanxi North Jindong Chemical Co., Ltd., Yangquan 045000, China

<sup>3</sup> China South Industries Group Co., Ltd., Beijing 100089, China

\* Correspondence: cqz1969@bit.edu.cn

**Abstract:** In this study, to solve the problem of low activity of aluminum nanoparticles in combustion, aluminum nanoparticles were coated with 2,2,4-trimethylpentane (C<sub>8</sub>H<sub>18</sub>-Al), enabling the deactivation of aluminum nanoparticles to be effectively inhibited. The morphological characteristics, particle size distribution, chemical state, and thermal properties of C<sub>8</sub>H<sub>18</sub>-Al were characterized via SEM, TEM, DLS, XPS, and TG-DSC. The stability and energy performance of C<sub>8</sub>H<sub>18</sub>-Al were studied based on the national standard test method. The results showed that C<sub>8</sub>H<sub>18</sub>-Al had a typical shell–core structure with a smooth surface and good sphericity. The particle size was normally distributed, and the content of active aluminum nanoparticles was high (85.45%), with good thermal stability and a fast energy release rate (about four times that of ordinary nano aluminum particles). The results demonstrated that an in situ C<sub>8</sub>H<sub>18</sub> coating is beneficial for the preparation of structurally stable aluminum nanoparticle composites with good performance.

**Keywords:** 2,2,4-trimethylpentane coated; aluminum nanoparticles; characterization; energy and stable performance



**Citation:** Wang, G.; Wang, H.; Cui, Q.; Li, X.; Wu, X.; Liao, H.; Zhang, Z. Synthesis, Analysis, and Characterization of Aluminum Nanoparticles Coated with 2,2,4-Trimethylpentane. *Metals* **2023**, *13*, 322. <https://doi.org/10.3390/met13020322>

Academic Editors: Frank Czerwinski and Leonid M. Kustov

Received: 26 December 2022

Revised: 28 January 2023

Accepted: 3 February 2023

Published: 5 February 2023



**Copyright:** © 2023 by the authors. Licensee MDPI, Basel, Switzerland. This article is an open access article distributed under the terms and conditions of the Creative Commons Attribution (CC BY) license (<https://creativecommons.org/licenses/by/4.0/>).

## 1. Introduction

Exploring the structure and properties of metal nanoparticles is imperative in research areas such as materials synthesis, catalysis, and combustion applications [1]. For aluminum nanoparticles, due to their high surface activity and high specific surface area properties [2], problems such as the deactivation of aluminum nanoparticles leading to reduced active aluminum nanoparticle content have created challenges in the combustion community. Therefore, in order to maintain the high activity of aluminum nanoparticles in practical applications, the surfaces of aluminum nanoparticles need to be treated. The main methods currently used to maintain the activity of aluminum nano powders are inert gas protection [3], natural passivation [4], and surface coating [5]. Among them, the surface coating method can effectively solve the problems of agglomeration and easy oxidation by forming a nanoscale core–shell structure and changing the surface functionalization properties of nano aluminum nanoparticles, which can effectively improve the combustion of aluminum nanoparticles [6].

Most coatings on the surfaces of aluminum nanoparticles are inorganic, including carbon [7,8], metal and oxide [4,9,10], and nonmetallic coatings [11]. Yi et al. [7] investigated the structural stability and thermal decomposition mechanisms of nanocarbon-material-coated aluminum powder particles, Al@C, and found that the core–shell structure of Al@C can provide effective protection for Al surface activity. Kou et al. [9] found that Fe/Al composites prepared via the one-step reduction method have a large specific surface area. The coated Fe has the ability to effectively reduce alumina, thus increasing the exothermic rate of Al nanoparticles. Sung et al. [11] prepared AlN particles via the plasma technique with high dispersion and kept the particle size smaller than that of the original Al

particles. However, lowering of the onset oxidation temperature and the poor compatibility of the components due to the inorganic coating of the aluminum nanoparticles led to reduced applicability. These factors limit the applications of aluminum nano powders in combustion.

In addition, coating materials are generally made from organic materials such as polymers [5,12], ether [13–15], and propellant components [16,17]. Kim et al. [12] prepared PTFE/Al using PTFE-coated aluminum nanoparticles with higher thermogravimetric enthalpy ( $4.80 \text{ kJg}^{-1}$ ) than that of pure Al powder ( $0.88 \text{ kJg}^{-1}$ ). A PTFE coating can also be used as an oxide layer to protect Al nanoparticles. Sun et al. [14] studied ether-coated Al nanoparticles using ReaxFF molecular dynamics and confirmed the presence of the ether coating through TEM of ECANPs with a thickness of 4.6 nm and concluded that the ether coating can effectively prevent the oxidation reaction of Al nanoparticles. Wang et al. [16] prepared Al/CuO/NC/AP composites via the electrospray method and found that ammonium perchlorate could improve the performance of Al/CuO nano alumina thermite.

There are other organic coatings that also serve to protect aluminum nanoparticles. To reduce the ignition temperature of Al nanoparticles, Zhang et al. [17] prepared Al@PFHP nanoparticles with a uniform structure and high sphericity with a lower ignition point ( $140 \text{ }^\circ\text{C}$  lower) and longer burning time (about 1.5 times more) compared to the original Al nanoparticles. Li et al. [18] comparatively studied the flame propagation behavior and minimum explosion concentration of AL and SA-Al and found that a stearic acid coating was able to suppress the explosion of aluminum nanoparticles. Organic materials are gradually attracting the interest of researchers as an ideal protective material because of their structural stability, insensitivity to water and air, and compatibility. 2,2,4-Trimethylpentane ( $\text{C}_8\text{H}_{18}$ ) [19,20] is stable and non-aggregating and is often applied as a standard for testing the anti-explosive properties of gasoline. Additionally, the high percentage of  $\text{C}_8\text{H}_{18}$  in the fuel mixture is considered to be able to reduce engine detonation [21].

Therefore, to avoid the oxidation reaction of aluminum nanoparticles easily in air, thereby reducing the energy release, in this study, 2,2,4-trimethylpentane was used for the in situ coating of aluminum nanoparticles, and morphological characterization and performance tests of the prepared coated samples were performed. The coating effects and properties of the 2,2,4-trimethylpentane coating material on aluminum nanoparticles were also investigated. As expected, 2,2,4-trimethylpentane was able to form a stable protective film on the aluminum nanoparticles indicated, thus effectively maintaining the high activity of aluminum nanoparticles and solving the problem of the limited application of aluminum nanoparticles in the combustion community.

## 2. Experiment

### 2.1. Materials

2,2,4-Trimethylpentane ( $\text{C}_8\text{H}_{18}$ ) was provided by China Sichuan Hongbo New Material Co., Ltd. (Mianyang, China). Aluminum wire (0.2 mm diameter, 99.5% purity) was supplied by China Shijiazhuang Zhongli Zinc Industry Co., Ltd. (Shijiazhuang, China). Ethanol and ethyl acetate (analytical purity) were supplied by Beijing Tongguang Fine Chemical Co., Ltd. (Beijing, China). Chemicals other than aluminum wire were directly used for in situ coating experiments without further treatment.

### 2.2. Fabrication of $\text{C}_8\text{H}_{18}$ -Al Nanoparticles

$\text{C}_8\text{H}_{18}$ -Al nanoparticles were prepared via the in situ coating of aluminum nanoparticles prepared via the electro-explosive by wire (EEW) method with 2,2,4-trimethylpentane. Aluminum vapor was generated by the separation explosion of aluminum wires (0.2 mm) in an explosion chamber with a transient high voltage (6.5 kv) supplied by the pulsed power generator. The distance between electrodes was 24 mm. Since the explosion chamber was filled with an inert gas (argon), the aluminum vapor collided with the gaseous medium and cooled rapidly, condensing into ultra-fine metal powder (aluminum nanoparticles). Subsequently, the prepared pure aluminum nanoparticles were collected by the separation unit-buffer tank-

powder collection unit and stored hermetically to avoid oxidation. To implement the in situ encapsulation of aluminum nanoparticles, 1 g of collected aluminum nanoparticles was taken and dispersed in a solution of ethyl acetate with a concentration of 10% ethanol.  $C_8H_{18}$  was added while stirring the solution until the aluminum nanoparticles were uniformly distributed in the solution. Then, the solution was placed in a fume hood until the volume evaporated completely. Finally, the black powder product coated with  $C_8H_{18}$  aluminum nanoparticles was screened. The products were collected and stored in a vacuum-tight environment for further morphological characterization and performance testing.

### 3. Characterization and Performance

#### 3.1. Equipment

The morphological structure of the  $C_8H_{18}$ -Al was analyzed via scanning electron microscopy (S4800 cold field emission SEM, Hitachi, Japan) and transmission electron microscopy (Tecnai G2 F20 FEM, FEI, Hillsboro, OR, USA). The particle size distribution of the sample was obtained from dynamic light scattering (Nanotracs Flex DLS, Microtrac Inc., Norcross, GA, USA). The chemical states of the constituent elements on the surface of the  $C_8H_{18}$ -Al were measured via X-ray photoelectron spectroscopy (Thermoescalab 250Xi XPS, Thermo Electron Corporation, Waltham, MA, USA). Analyses of the slow heating process of the samples were carried out via thermogravimetric analysis and differential scanning calorimetry (STA229F3 TG-DSC, Netzsch, Germany). The energy performance of  $C_8H_{18}$ -Al was characterized by a microcomputer automatic calorimeter (TRHW-7000C, Hebi Tianrun Technology Co., Ltd., Hebi, China).

#### 3.2. Morphology Analysis

The prepared  $C_8H_{18}$ -Al samples were uniformly coated with conductive resin and sprayed with gold to obtain the surface samples for SEM measurement. The different magnifications of the  $C_8H_{18}$ -Al samples are shown in Figure 1a (magnification 25.0K) and Figure 1b (magnification 100K) in order to highlight the grain sizes and compare them. The test results of the  $C_8H_{18}$ -Al samples showed that the  $C_8H_{18}$ -Al nanoparticles were spherical in shape with regular forms and relatively smooth-looking surface textures. Most of the nanoparticles were less than 200 nm in size, but a few larger particles were still present in the field of view due to interparticle aggregation and the stacking of clusters.

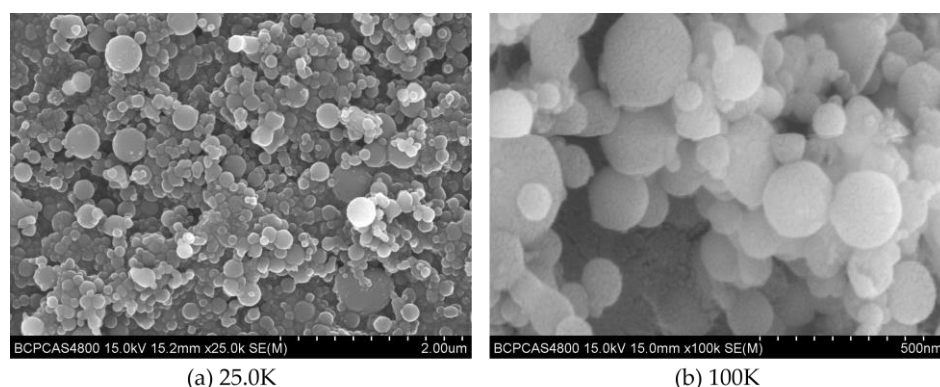


**Figure 1.** SEM image of  $C_8H_{18}$ -Al nanoparticles: (a) magnification 25.0 K, (b) magnification 100 K.

The imaging principle is basically the same for both SEM and TEM. SEM is able to observe only the surface morphology of the sample, while the electron beam of TEM is able to penetrate a certain thickness (about 50 nm) of the sample. Meanwhile, due to the different densities of the nanoscale aluminum particles and the shell structure of  $C_8H_{18}$ , the photographic results exhibited different gray levels. The milled  $C_8H_{18}$ -Al nanoparticle samples were dispersed in an anhydrous ethanol solution, sonicated, and then dropped on the microgrid and dried to produce samples for the TEM test. The TEM test results for the  $C_8H_{18}$ -Al nanoparticles are shown in Figure 2a. Here, it can be seen that brief

ultrasonic oscillation alleviated the agglomeration phenomenon of  $C_8H_{18}$ -Al nanoparticles. The particles were intact in shape with smooth edges, indicating the structural stability of the in situ  $C_8H_{18}$  coating.

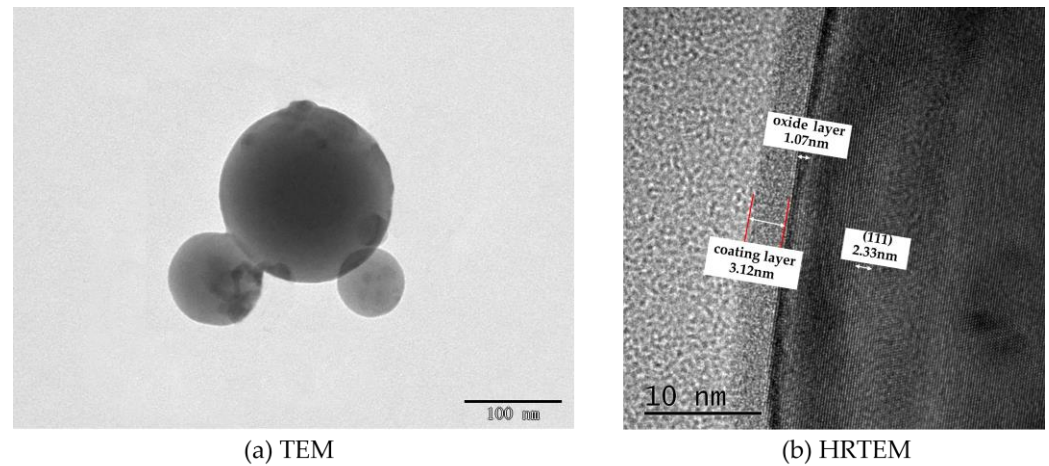


**Figure 2.** TEM image of  $C_8H_{18}$ -Al nanoparticles.

To gain insight into the interfacial information between the  $C_8H_{18}$  coating and the Al nanoparticles, HRTEM imaging of the  $C_8H_{18}$ -Al nanoparticles was performed in order to visually measure the thickness of the coating. The  $C_8H_{18}$ -Al nanoparticles clearly presented a typical core-shell structure with well-defined boundaries. The shell-core interface structure is controlled by the  $C_8H_{18}$  shell structure, the shell is dense and complete, there is no diffraction stripe at the inner side of the interface, and the cladding thickness is about 3.12 nm. A thin oxide layer (1.07 nm) was also visible, and no obvious crystal structure was seen in the field of view, indicating an amorphous alumina structure. The core of  $C_8H_{18}$ -Al nanoparticles has a distinct lattice stripe with a measured lattice spacing of 0.233 nm, which corresponds to the (111) face of the face-centered cubic Al [21]. Moreover, the  $C_8H_{18}$ -Al nanoparticles prepared by this method can effectively reduce the thickness of the oxide layer [16].

### 3.3. Particle Size Analysis

It is necessary to know the particle size distribution of  $C_8H_{18}$ -Al samples because smaller aluminum nanoparticles are theoretically more conducive to a positive combustion reaction [22]. Dynamic light scattering (DLS) has been widely used as an inexpensive and fast particle size determination method for metal particle size measurement [23]. We dispersed 1.0 mg of the  $C_8H_{18}$ -Al sample in 150 mL of ethanol and shook it via ultrasound before testing to ensure the precision of the measurement results. The particle size distribution of the  $C_8H_{18}$ -Al particles was analyzed using statistical methods, as shown in Figure 3. The median particle size D50 of  $C_8H_{18}$ -Al nanoparticles was greater than 200 nm, while D95 was equal to 310 nm, which is generally consistent with the conclusions obtained from the SEM observations. The particle size distribution of the samples showed an overall normal distribution and more concentrated particle size distribution. This result indicated that the overall homogeneity of the samples with in situ coating of nano Al powder with  $C_8H_{18}$  performed better.

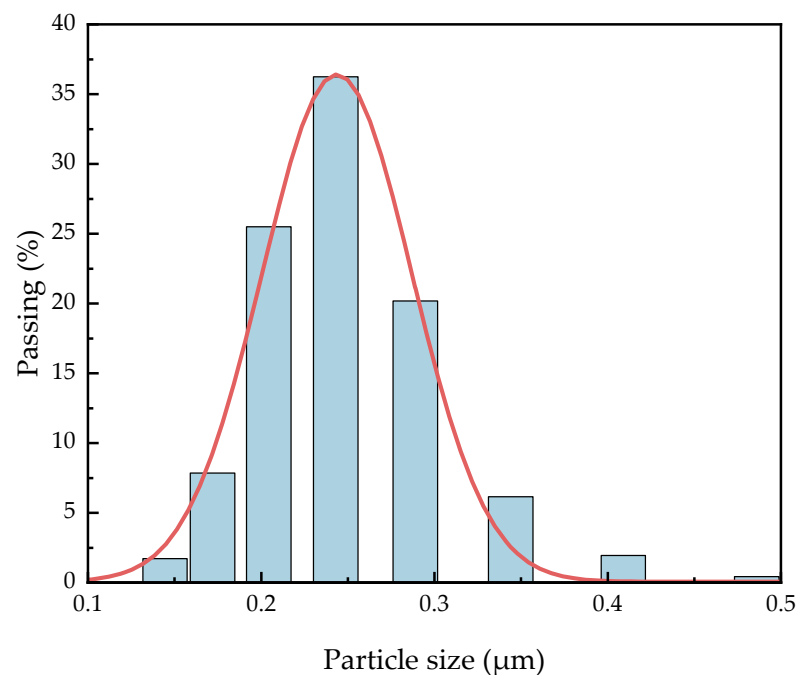


**Figure 3.** Particle size distribution of C<sub>8</sub>H<sub>18</sub>-Al nanoparticles.

### 3.4. Active Aluminum Content Analysis

Nano aluminum powder theoretically has higher reactivity than micron aluminum powder, but the active aluminum content decreases dramatically with decreasing particle size because nano aluminum powder offers easy oxidation. It is necessary to understand the effect of the level of active aluminum content on combustion performance [24]. In order to characterize the content of active aluminum of the coated samples, the content of active aluminum was obtained by calculating the volume of hydrogen gas released from the reaction of active aluminum with sodium hydroxide according to the gas volume method of YS/T 617.1-2007 [18] using Formula (1); the specific experimental methods and equipment are not described here. Simultaneously, to illustrate how effective the C<sub>8</sub>H<sub>18</sub>-coated nano Al powder was, the results were compared with two sizes and types of Al powder (ordinary nano Al and micro Al), as shown in Table 1. We observed that the content of the three active Al samples, from high to low, was micro Al > C<sub>8</sub>H<sub>18</sub>-Al > ordinary nano Al, which also indicated that the aluminum powder was inevitably oxidized during the preparation of C<sub>8</sub>H<sub>18</sub>-Al. The activity of aluminum powder coated with C<sub>8</sub>H<sub>18</sub> was greater than 80%, which was much higher than the activity of ordinary aluminum powder (59.18%), and the active aluminum content increased by 26.27%, which indicated that the coating layer protected the active aluminum in the inner layer very well.

**Table 1.** Testing results of active Al content.

Sample	Active Al Content (%)
C <sub>8</sub> H <sub>18</sub> -Al	85.45
Ordinary nano Al [25]	59.18
Micro Al [25]	90.73

$$\omega_{\text{active Al content}} = \frac{0.00216(P_m - P_b - P_s) \times V}{(273 + t)m_0} \times 100\% \quad (1)$$

where  $P_m$  is the mercury air pressure display value (kPa),  $P_b$  is the corrected value of the barometer display temperature (kPa),  $P_s$  is the saturation vapor pressure of water when the temperature is measured (kPa),  $m_0$  is the mass of the sample (g),  $V$  is the volume of hydrogen

gas produced (mL), 0.00216 is the conversion factor for converting hydrogen into active aluminum, and  $t$  is the temperature in the measuring tube at the time of measurement ( $^{\circ}\text{C}$ )

### 3.5. X-ray Electron Spectroscopy (XPS) Analysis

X-ray photoelectron spectroscopy (XPS) is capable of qualitative and semi-quantitative analysis of the chemical state and electronic structure of elements on the surface of solid materials (<5 nm). Since the sample itself contains elemental carbon, the 2 mg powder sample was glued to an ordinary double-sided adhesive. The  $\text{C}_8\text{H}_{18}\text{-Al}$  nanoparticles were dried to avoid solvent influence on the analysis results, and characterization was performed. The total spectrum was analyzed via inverse fold product analysis using the XPS PEAK software which is Avantage (Thermo Scientific, Waltham, MA, USA). No elemental signals were detected besides the presence of C, O, and Al, which were labeled. The results are shown in Figure 4.

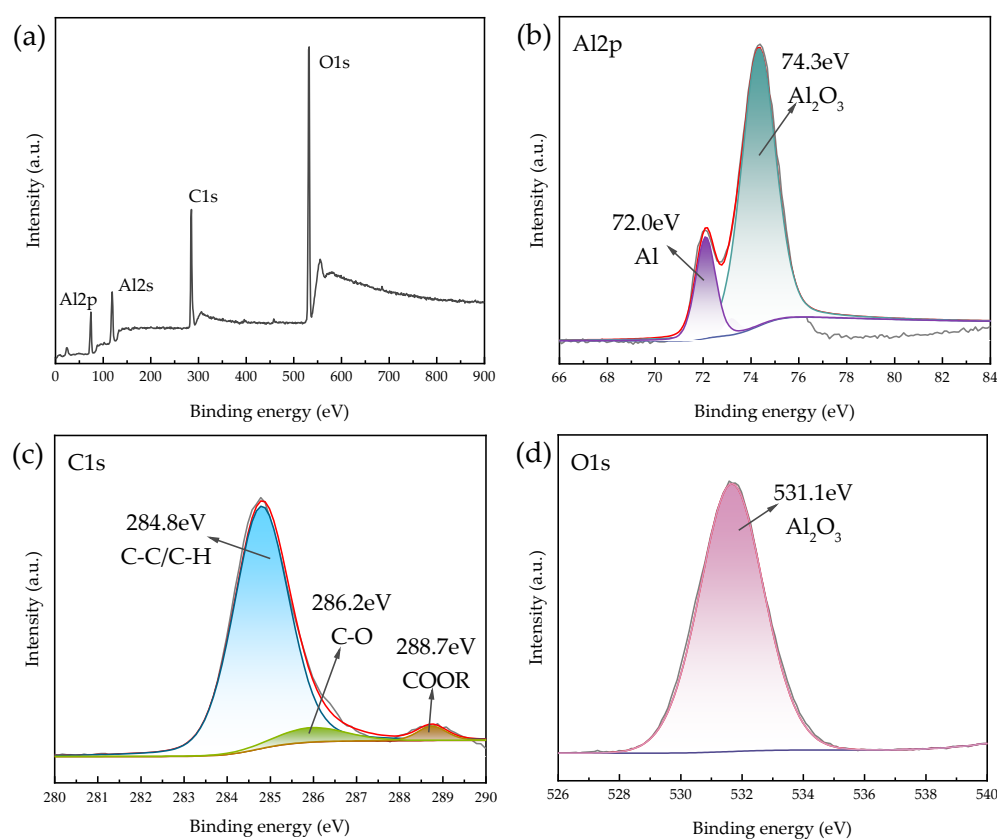


**Figure 4.** XPS spectra of  $\text{C}_8\text{H}_{18}\text{-Al}$  nanoparticles: (a) XPS full-scan spectrum, (b) Al2p, (c) C1s, and (d) O1s.

The Al2s spectrum shown in Figure 4a presents residual  $\text{Al}_2\text{O}_3$  compounds at 120.2 eV [26] and is not described in detail here. Two chemical states,  $\text{Al}_2\text{O}_3$  (74.3 eV) and singlet Al (72.0 eV), can be seen in Figure 4b [26], which proves the presence of a partial oxide layer of aluminum on the surface of the  $\text{C}_8\text{H}_{18}\text{-Al}$  sample during in situ cladding, as well as the sample processing measurements. The C1s envelope for the  $\text{C}_8\text{H}_{18}\text{-Al}$  control was deconvoluted into three peaks representing four types of carbon that correspond to C-C/C-H (284.8 eV), C-O (286.2 eV), and O=C-OR/O=C-OH (288.7 eV) [27,28]. This result indicates that part of the  $\text{C}_8\text{H}_{18}$  was oxidized during the coating process, forming hydroxyl, carbonyl, and carboxyl functions. This coating then becomes a new oxide layer that is similar to aluminum oxide on the surface of aluminum nanoparticles. Based on the Al2p, C1s, and O1s spectra, we confirmed that the  $\text{C}_8\text{H}_{18}$  coating was encapsulated in the periphery of the aluminum nanoparticles [9].

### 3.6. Thermal Analysis

TG-DSC studies were performed on C<sub>8</sub>H<sub>18</sub>-Al nanoparticles under an air atmosphere at a heating rate temperature of 20 °C/min from 23 to 1350 °C to study the conversion process, and the results are shown in Figure 5. The TG-DSC curves of C<sub>8</sub>H<sub>18</sub>-Al nanoparticles were analyzed with reference to the temperature dependence of C<sub>8</sub>H<sub>18</sub> and its decomposition products [20] and the oxidation stage curves of micro-nano alumina powders [29,30]. According to the trend of the TG curve, the mass of C<sub>8</sub>H<sub>18</sub>-Al nanoparticles was divided into four stages with temperature, and the reasons for the changes were analyzed in conjunction with the DSC curves as follows:

1. From 23 to 400 °C, the sample mass decreased by about 4.6%. Since amorphous alumina is hydrophilic [30], the increase in temperature leads to desorption of H<sub>2</sub>O and CO<sub>2</sub> attached to the surface. At the same time, some of the amorphous carbon on the nanoparticle surface was oxidized into CO<sub>2</sub> spillover [31]. The thickening of the amorphous oxide layer Al<sub>2</sub>O<sub>3</sub> of the shell structure occurred at this stage.
2. The sample mass gradually increased by about 27.4% from 400 to 693 °C. The exothermic peak at 593 °C on the DSC curve was the first oxidative exothermic peak, and the integration yielded an exotherm of 2.98 kJ/g. A phase change peak caused by the melting of unreacted aluminum appeared at 647.5 °C. The oxidation onset temperature on the TG curve was 554.2 °C, at which point the amorphous Al<sub>2</sub>O<sub>3</sub> started to convert into  $\gamma$ -Al<sub>2</sub>O<sub>3</sub>. The subsequent flat weight gain was due to the alumina shell hindering the contact of aluminum with oxygen to reduce the probability of oxidation reaction. In addition, as the temperature increased, the molten aluminum destroyed the oxide layer, and the eruption of reactive aluminum caused the internal alumina nanoparticles to begin oxidation. Meanwhile, this phase of C<sub>8</sub>H<sub>18</sub> was oxidized and decomposed to produce a series of olefins (C<sub>4</sub>H<sub>8</sub>, CH<sub>4</sub>, C<sub>2</sub>H<sub>2</sub>, and C<sub>3</sub>H<sub>6</sub>) [20].
3. The temperature varied between 693 and 945 °C. The oxidation reaction of aluminum nanoparticles occurred predominantly at this stage [29], and the mass of the sample increased by 25.6%. The second exothermic peak on the DSC curve at 806.2 °C corresponded to the conversion of  $\gamma$ -Al<sub>2</sub>O<sub>3</sub> to  $\theta$ -Al<sub>2</sub>O<sub>3</sub>, which was calculated to be 2.72 kJ/g. The decomposition of C<sub>8</sub>H<sub>18</sub> at this phase was basically complete [20].
4. The temperature increased from 945 °C to the end of the ramp-up, by which time most of the Al nanoparticles were almost completely oxidized. The TG curve showed that there was still a mass change, which corresponded to a small exothermic peak at 1051.8 °C on the DSC curve, indicating that there was still an unreacted aluminum nanoparticle. After this point, the weight gain stopped, and  $\theta$ -Al<sub>2</sub>O<sub>3</sub> transformed into stably present  $\alpha$ -Al<sub>2</sub>O<sub>3</sub>. The final C<sub>8</sub>H<sub>18</sub>-Al nanoparticles gained 67.3% in weight, with a total exothermic heat of 24.8 kJ/g.

A comparison with the measured results of different types of aluminum powder raw materials under similar test conditions (ordinary nano Al and micro Al) is shown in Table 2. The order for the onset oxidation temperature from high to low was ordinary nano Al > micro Al > C<sub>8</sub>H<sub>18</sub>-Al, indicating that the C<sub>8</sub>H<sub>18</sub>-Al nanoparticles with higher reactivity and earlier reactions were able to accelerate the reaction rate of aluminum powder in the high-temperature gas phase environment. The order for the weight gain of nanoparticle samples from high to low was micron Al > C<sub>8</sub>H<sub>18</sub>-Al > ordinary nano Al. This result indicates that the active aluminum content of C<sub>8</sub>H<sub>18</sub> nanoparticles may be between micron aluminum powder and normal nano aluminum powder, thereby confirming the results of the active aluminum content test.

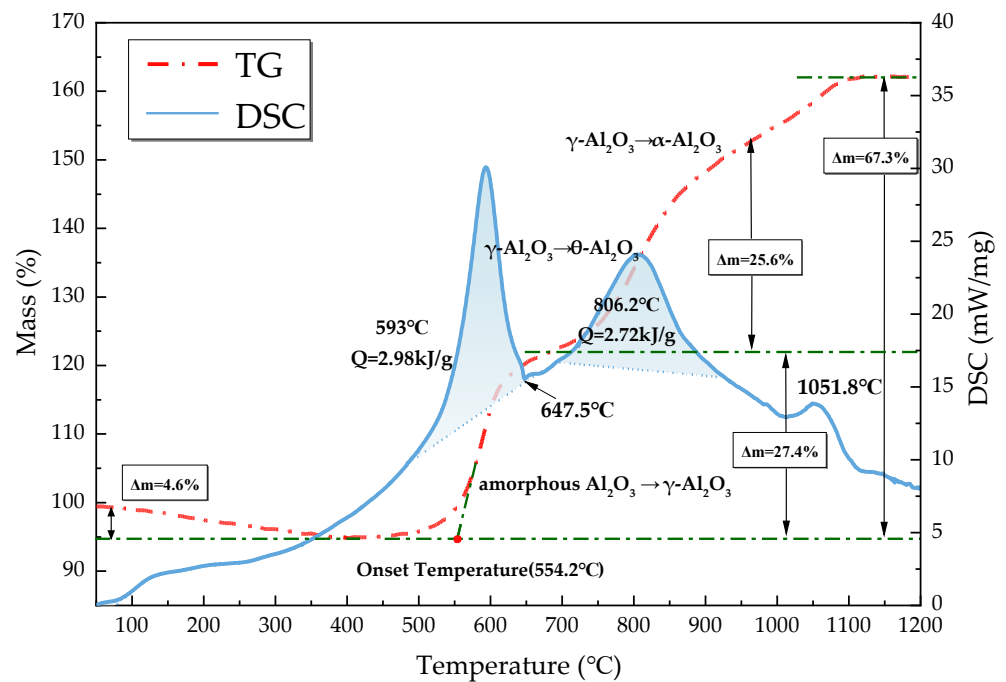


**Figure 5.** TG-DSC curves of  $C_8H_{18}$ -Al nanoparticles.

**Table 2.** Thermal analysis data of three samples.

Sample	Onset Temperature (°C)	Weight Gain ( $\Delta m$ %)
$C_8H_{18}$ -Al	554.2	67.3
Ordinary nano Al [25]	567.0	57.0
Micro Al [25,32]	555.7	81.0

### 3.7. Stability Performance

The thermal stability test of the  $C_8H_{18}$ -Al sample was carried out via the heating method at  $75^\circ\text{C}$  with reference to part XIII of GJB5891.13-2006 [33]. The specimen vials containing 1.0 g of  $C_8H_{18}$ -Al nanoparticles were placed in an oven and heated continuously at  $75 \pm 2^\circ\text{C}$  for 48 h. A set heating temperature was used to evaluate the thermal stability of the sample by calculating the mass fraction reduction of the sample over a period of time according to Equation (2). The two sets of parallel tests were conducted on the  $C_8H_{18}$ -Al test sample, and the average value was taken for the two test cases with a difference of no more than 0.02% to obtain the weight loss mass fraction of the  $C_8H_{18}$ -Al sample:  $0.55\% \pm 0.11\%$ . The results indicated that the state of the coating layer of  $C_8H_{18}$ -Al nanoparticles was stable, and that the color of the samples did not change significantly before and after heating. Additionally, the samples had good thermal stability, which indicated that the coating layer could protect the nano aluminum powder well.

$$W = \frac{m_0 - m_1}{m} \times 100\% \quad (2)$$

where  $W$  is the mass fraction of the sample reduction (%),  $m_0$  is the total mass of the specimen vessel and specimen before heating (g),  $m_1$  is the total mass of the specimen vessel and specimen after heating (g), and  $m$  is the mass of the sample weighed.

The vacuum stability of the sample was tested using the pressure sensor method based on GJB772A-97 (501.2) [34]. Pretreatment of the  $C_8H_{18}$ -Al test sample was carried out with drying at  $55^\circ\text{C}$  for 2 h before the experiment to avoid water molecules and alkane solvent molecules from affecting the test results. The vacuum stability test was conducted by weighing  $1 \pm 0.01$  g of the pretreatment sample, and the average value was taken from

three parallel tests. The gas yield of the experimental result for the C<sub>8</sub>H<sub>18</sub>-Al sample was  $1.301 \pm 0.132$  mL/g, calculated according to Equation (3), which was less than the 2 mL/g specified in the national standard, indicating that the stability of C<sub>8</sub>H<sub>18</sub>-Al was sufficient:

$$V_s = 2.69 \times 10^{-3} \frac{P_r}{T_a} (V_1 - V_0) \quad (3)$$

where  $V_s$  is the volume of gas released from the specimen in the standard state (mL),  $2.69 \times 10^{-3}$  is the ratio of the temperature to pressure under standard conditions (K/Pa),  $P_r$  is the pressure of the gas released from the specimen (Pa),  $T_a$  is the experimental ambient temperature (K),  $V_1$  is the sum of the reactor volume and the pressure measurement connection line volume (mL), and  $V_0$  is the volume of the specimen (mL).

### 3.8. Energy Performance

In addition to analyzing the morphological characteristics and chemical state of the coating material, it is necessary to understand the effects of the combustion performance of the coating sample. The heat from the combustion of C<sub>8</sub>H<sub>18</sub>-Al nanoparticles was determined and compared using a fully automatic calorimeter under program control based on GJB 770B-2005 (703.1) [34]. To guarantee the accuracy of the test, each sample was tested three times in parallel, averaged, and compared with aluminum powder. The results are shown in Table 3. The heat from the combustion of the samples was, from high to low, micro Al > C<sub>8</sub>H<sub>18</sub>-Al > ordinary nano Al, which agrees with the results of the active aluminum content test.

**Table 3.** Combustion heat of samples.

Sample	Combustion (MJ/kg)
C <sub>8</sub> H <sub>18</sub> -Al	26.41 ± 0.13
Ordinary nano Al [5]	19.69 ± 0.14
Micro Al [5,24]	28.40 ± 0.12

To further evaluate the energy generated by the combustion of C<sub>8</sub>H<sub>18</sub>-Al and the speed of the reaction, the differential pressure method was used to perform a confined exploder test to record the pressure generated during the combustion of C<sub>8</sub>H<sub>18</sub>-Al samples as a function of time. As shown in Figure 6, the maximum value of combustion pressure was 0.232 Mpa, and the maximum value of the pressure increase rate was 137 Mpa/s. Table 4 shows that the maximum pressure value for combustion of the C<sub>8</sub>H<sub>18</sub>-Al sample was higher than that of the micron aluminum powder and close to that of common nano aluminum powder. Nevertheless, the combustion rate of the C<sub>8</sub>H<sub>18</sub>-Al sample was about four times higher than that of the micron aluminum powder and normal nano aluminum powder. The results demonstrated that using C<sub>8</sub>H<sub>18</sub> as a coating layer can enable aluminum powder to release energy rapidly. The test results for the heat of combustion were also verified.

**Table 4.** Combustion performance comparison of samples.

Sample	P (Mpa)	(Mpa/s)
C <sub>8</sub> H <sub>18</sub> -Al	0.232	137
Ordinary nano Al [5]	0.238	34.1
Micro Al [5]	0.169	32.8

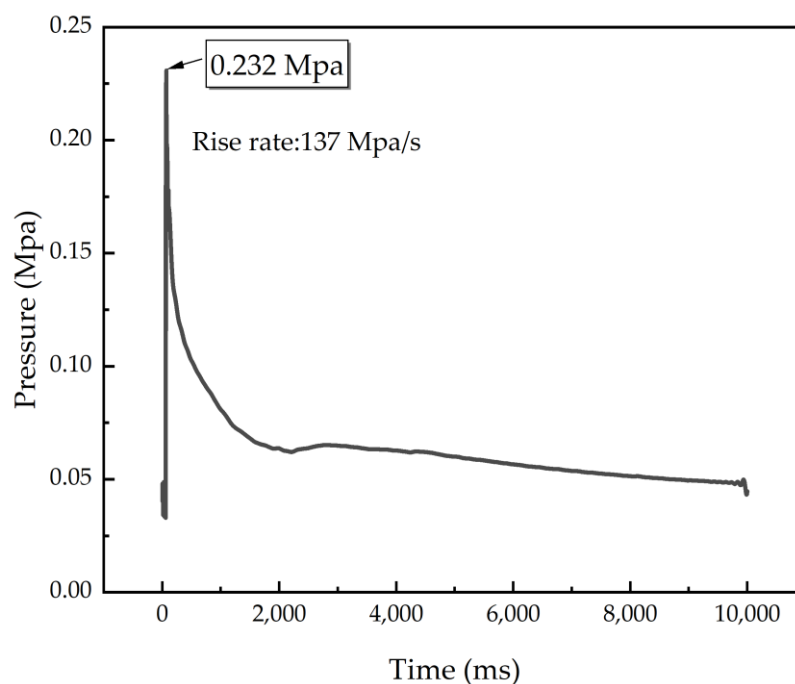


**Figure 6.** P–t curve of C<sub>8</sub>H<sub>18</sub>-Al nanoparticles.

#### 4. Conclusions

In this paper, C<sub>8</sub>H<sub>18</sub>-Al nanoparticles were synthesized for the first time by the in situ coating of aluminum nanoparticles with 2,2,4-trimethylpentane. The morphological characteristics, particle size distribution, chemical state, and thermal properties of the C<sub>8</sub>H<sub>18</sub>-Al nanoparticles were analyzed and characterized. C<sub>8</sub>H<sub>18</sub>-Al nanoparticles have a typical spherical shell–core structure with uniformity, and the shell structure consists of a 3.12 nm thick coating and a 1.07 nm thick oxide layer. The particle size was normally distributed, and the median particle size was 219.3 nm. The active aluminum content was 85.45%, which was better than the result for normal aluminum nanoparticles but lower than that of micron-sized aluminum particles. The XPS results confirmed the presence of C<sub>8</sub>H<sub>18</sub>, which combined with alumina to form hydroxyl, carboxyl, and carbonyl functional groups on the surface of the aluminum nanoparticles. The presence of amorphous alumina in C<sub>8</sub>H<sub>18</sub>-Al affected the thermal properties and burning rate of C<sub>8</sub>H<sub>18</sub>-Al. Stability experiments confirmed that the C<sub>8</sub>H<sub>18</sub> coating was not easily decomposed and could better protect the aluminum nanoparticles. The energy test results illustrated that C<sub>8</sub>H<sub>18</sub> as a cladding layer can make aluminum nanoparticles release energy rapidly (about four times more rapidly than normal aluminum nanoparticles). In summary, the results showed that the in situ coating of aluminum nanoparticles with 2,2,4-trimethylpentane is an effective method to ensure the presence of active aluminum content.

**Author Contributions:** Conceptualization, G.W. and H.W.; methodology, G.W. and H.W.; formal analysis, G.W. and Q.C.; investigation, X.L. and X.W.; data curation, H.L. and Z.Z.; writing—original draft preparation, G.W. and H.W.; writing—review and editing, G.W. and Q.C. All authors have read and agreed to the published version of the manuscript.

**Funding:** National Natural Science Foundation No. 21975024.

**Institutional Review Board Statement:** Not applicable.

**Informed Consent Statement:** Not applicable.

**Data Availability Statement:** The data presented in this study are available on request from the corresponding author.

**Conflicts of Interest:** The authors declare no conflict of interest.

## References

1. Subhan, A.; Mourad, A.-H.I.; Al-Douri, Y. Influence of Laser Process Parameters, Liquid Medium, and External Field on the Synthesis of Colloidal Metal Nanoparticles Using Pulsed Laser Ablation in Liquid: A Review. *Nanomaterials* **2022**, *12*, 2144. [[CrossRef](#)]
2. Sundaram, D.S.; Yang, V.; Zarko, V.E. Combustion of Nano Aluminum Particles (Review). *Combust. Explos. Shock. Waves* **2015**, *51*, 173–196. [[CrossRef](#)]
3. Zhang, S.; Bi, M.; Jiang, H.; Gao, W. Suppression Effect of Inert Gases on Aluminum Dust Explosion. *Powder Technol.* **2021**, *388*, 90–99. [[CrossRef](#)]
4. Kim, K.T.; Kim, D.W.; Kim, S.H.; Kim, C.K.; Choi, Y.J. Synthesis and Improved Explosion Behaviors of Aluminum Powders Coated with Nano-Sized Nickel Film. *Appl. Surf. Sci.* **2017**, *415*, 104–108. [[CrossRef](#)]
5. Wang, H.-X.; Ren, H.; Cui, Q.; Yan, T.; Li, Y.-R. Energy Release Prediction and Structure Characterization of Nano Aluminum Powder in Situ Coated by Polyethylene Glycol. *Ferroelectrics* **2020**, *563*, 161–176. [[CrossRef](#)]
6. Cohen, O.; Michaels, D.; Yavor, Y. Agglomeration in Composite Propellants Containing Different Nano-Aluminum Powders. *Propellants Explos. Pyrotech.* **2022**, *47*, e202100320. [[CrossRef](#)]
7. Yi, Q.; Xu, J.; Liu, Y.; Zhai, D.; Zhou, K.; Pan, D. Molecular Dynamics Study on Core-Shell Structure Stability of Aluminum Encapsulated by Nano-Carbon Materials. *Chem. Phys. Lett.* **2017**, *669*, 192–195. [[CrossRef](#)]
8. Hong, S.; van Duin, A.C.T. Atomistic-Scale Analysis of Carbon Coating and Its Effect on the Oxidation of Aluminum Nanoparticles by ReaxFF-Molecular Dynamics Simulations. *J. Phys. Chem. C* **2016**, *120*, 9464–9474. [[CrossRef](#)]
9. Kou, Y.; Wang, Y.; Zhang, J.; Guo, K.; Song, X. Iron/Aluminum Nanocomposites Prepared by One-Step Reduction Method and Their Effects on Thermal Decomposition of AP and AN. *Def. Technol.* **2021**. [[CrossRef](#)]
10. Ali, R.; Ali, F.; Zahoor, A.; Shahid, R.N.; Tariq, N.U.H.; Ali, G.; Ullah, S.; Shah, A.; Awais, H.B. Preparation and Oxidation of Aluminum Powders with Surface Alumina Replaced by Iron Coating. *J. Energ. Mater.* **2022**, *40*, 243–257. [[CrossRef](#)]
11. Sung, M.-C.; Wang, Y.-F.; Chen, S.-C.; Tsai, C.-H. Two-Stage Plasma-Thermal Nitridation Processes for the Production of Aluminum Nitride Powders from Aluminum Powders. *Materials* **2019**, *12*, 359. [[CrossRef](#)] [[PubMed](#)]
12. Kim, K.T.; Kim, D.W.; Kim, C.K.; Choi, Y.J. A Facile Synthesis and Efficient Thermal Oxidation of Polytetrafluoroethylene-Coated Aluminum Powders. *Mater. Lett.* **2016**, *167*, 262–265. [[CrossRef](#)]
13. Liu, P.; Sui, P.; Feng, Z.; Gao, S.; Song, N.; Sun, R. Molecular Dynamic Investigations of Aluminum Nanoparticles Coated by the Mixtures of Ethanol and Diethyl Ether with Different Molecular Proportions. *J. Nanoparticle Res.* **2020**, *22*, 240. [[CrossRef](#)]
14. Sun, R.; Liu, P.; Qi, H.; Liu, J.; Ding, T. Molecular Dynamic Simulations of Ether-Coated Aluminum Nano-Particles as a Novel Hydrogen Source. *J. Nanopart. Res.* **2019**, *21*, 72. [[CrossRef](#)]
15. Ye, M.; Zhang, S.; Liu, S.; Han, A.; Chen, X. Preparation and Characterization of Pyrotechnics Binder-Coated Nano-Aluminum Composite Particles. *J. Energ. Mater.* **2017**, *35*, 300–313. [[CrossRef](#)]
16. Wang, C.; Xu, J.; Dai, J.; Wang, Y.; Shen, Y.; Zhang, Z.; Shen, R.; Ye, Y. Probing the Reaction Mechanism of Al/CuO Nanocomposites Doped with Ammonium Perchlorate. *Nanotechnology* **2020**, *31*, 255401. [[CrossRef](#)]
17. Zhang, L.; Wang, S.; Su, X.; Li, X.; Zou, M. Preparation and Characterization of Core-Shell Al@PFHP with Improving the Combustion and Ignition Properties of Aluminum Powder. *Particuology* **2023**, *77*, 62–70. [[CrossRef](#)]
18. Li, N.; Zhang, Y.; Guo, R.; Yang, J.; Zhang, X.; Wang, X. Effect of Stearic Acid Coating on the Explosion Characteristics of Aluminum Dust. *Fuel* **2022**, *320*, 123880. [[CrossRef](#)]
19. Westrich, T.A.; Chen, X.; Schwank, J.W. Isooctane Decomposition and Carbon Deposition over Ceria–Zirconia Supported Nickel Catalysts. *Appl. Catal. Gen.* **2010**, *386*, 83–93. [[CrossRef](#)]
20. Guan, Y.; Gao, Y.; Lou, J.; Zhu, X.; Pan, D.; Ma, H. High-Temperature Thermal Decomposition of Iso-Octane Based on Reactive Molecular Dynamics Simulations. *J. Mol. Model.* **2022**, *28*, 124. [[CrossRef](#)] [[PubMed](#)]
21. Ogawa, F.; Masuda, C. Interface Observation of Aluminum-Coated Carbon Nanofibers Prepared by in Situ Chemical Vapor Deposition. *J. Phys. Chem. C* **2017**, *121*, 6126–6132. [[CrossRef](#)]
22. Xiao, F.; Gao, W.; Li, J.; Yang, R. Effect of the Aluminum Particle Size, Solid Content, and Aluminum/Oxygen Ratio on the Underwater Explosion Performance of Aluminum-Based Explosives. *Combust. Explos. Shock Waves* **2020**, *56*, 576–584. [[CrossRef](#)]
23. National Development and Reform Commission of the People’s Republic of China. *Determination of Chemical Compositions and Physical Properties of Aluminum Powder, Magnesium Powder and Al-Mg Alloy Powder—Part 1: Determination of Active Al, Mg or Al-Mg Content—Gasometric Method*; National Development and Reform Commission of the People’s Republic of China: Beijing, China, 2007; Volume YS/T 617.1-2007, pp. 1–3.
24. Wang, H.; Ren, H.; Yan, T.; Li, Y. Micro-structure and Active Aluminum Content of Aluminum Powder in Situ Coated by Polyvinyl Alcohol. *Acta Armamentarii* **2019**, *40*, 1373–1380.
25. Gall, S.; Manuel, S.; Lerat, J.-F. Boron Laser Doping through High Quality Al<sub>2</sub>O<sub>3</sub> Passivation Layer for Localized B-BSF PERL Solar Cells. *Energy Procedia* **2013**, *38*, 270–277. [[CrossRef](#)]
26. McMahan, B.W.; Perez, J.P.L.; Yu, J.; Boatz, J.A.; Anderson, S.L. Anderson Synthesis of Nanoparticles from Malleable and Ductile Metals Using Powder-Free, Reactant-Assisted Mechanical Attrition. *ACS Appl. Mater. Interfaces* **2014**, *6*, 19579–19591. [[CrossRef](#)]
27. Song, Y.; Zhen, W.; Han, W.; Zhou, Y.; Sun, J. Polymethylmethacrylate Grafting onto Polyvinyl Alcohol/Modified Feldspar Composites: Preparation, Properties and Structure Characterization. *Iran. Polym. J.* **2014**, *23*, 375–386. [[CrossRef](#)]

28. Saceleanu, F.; Atashin, S.; Wen, J.Z. Investigation of the Effects of Phase Transformations in Micro and Nano Aluminum Powders on Kinetics of Oxidation Using Thermogravimetric Analysis. *Phys. Chem. Chem. Phys.* **2017**, *19*, 18996–19009. [[CrossRef](#)] [[PubMed](#)]
29. Noor, F.; Zhang, H.; Korakianitis, T.; Wen, D. Oxidation and Ignition of Aluminum Nanomaterials. *Phys. Chem. Chem. Phys.* **2013**, *15*, 20176–20188. [[CrossRef](#)]
30. Abdelkader, E.M.; Jelliss, P.A.; Buckner, S.W. Main Group Nanoparticle Synthesis Using Electrical Explosion of Wires. *Nano-Struct. Nano-Objects* **2016**, *7*, 23–31. [[CrossRef](#)]
31. Cheng, Y.Z.; Ren, H.; Li, Y.-R.; Jiao, Q.-J. Fluorine-coated High Reactive Al with Modified Metal Electric Explosion Wire Method. *Chin. J. Explos. Propellants* **2021**, *44*, 753–760.
32. Commission for Science, Technology and Industry for National Defense. *Test Method of Loading Material for Initiating Explosive Device—Part 13: Heat Endurance Test—Method of 75 °C Heat*; Commission for Science, Technology and Industry for National Defense: Beijing, China, 2006; Volume GJB 5891.13-2006.
33. Commission for Science, Technology and Industry for National Defense. *Explosive Test Method*; Commission for Science, Technology and Industry for National Defense: Beijing, China, 1997; Volume GJB 772A-97.
34. Commission for Science, Technology and Industry for National Defense. *Test Method of Propellant*; Commission for Science, Technology and Industry for National Defense: Beijing, China, 2005; Volume GJB 770B-2005, pp. 304–312.

**Disclaimer/Publisher’s Note:** The statements, opinions and data contained in all publications are solely those of the individual author(s) and contributor(s) and not of MDPI and/or the editor(s). MDPI and/or the editor(s) disclaim responsibility for any injury to people or property resulting from any ideas, methods, instructions or products referred to in the content.